Eur Biophys J (2009) 39:111–120
DOI 10.1007/s00249-009-0433-1

ORIGINAL PAPER

Structure of the pore-helix of the hERG K^+ channel

Guilhem Pages · Allan M. Torres · Pengchu Ju · Paramjit S. Bansal · Paul F. Alewood · Philip W. Kuchel · Jamie I. Vandenberg

Received: 27 January 2009 / Revised: 19 February 2009 / Accepted: 23 February 2009 / Published online: 21 March 2009

Abstract The hERG K^+ channel undergoes rapid inactivation that is mediated by 'collapse' of the selectivity filter, thereby preventing ion conduction. Previous studies have suggested that the pore-helix of hERG may be up to seven residues longer than that predicted by homology with channels with known crystal structures. In the present work, we determined structural features of a peptide from the pore loop region of hERG (residues 600–642) in both sodium dodecyl sulfate (SDS) and dodecyl phosphocholine (DPC) micelles using NMR spectroscopy. A complete structure calculation was done for the peptide in DPC, and the localization of residues inside the micelles were analysed by using a water-soluble paramagnetic reagent with both DPC and SDS micelles. The pore-helix in the hERG peptide was only two–four residues longer at the N-terminus, compared with the pore helices seen in the crystal structures of other K^+ channels, rather than the seven residues suggested from previous NMR studies. The helix in the peptide spanned the same residues in both micellar environments despite a difference in the localization inside the respective micelles. To determine if the extension of the length of the helix was affected by the hydrophobic environment in the two types of micelles, we compared NMR and X-ray crystallography results from a homologous peptide from the voltage gated potassium channel, KcsA.

Keywords *Human ether-a-go-go related* gene · NMR spectroscopy · Paramagnetic relaxant reagent · Voltage-gated potassium channels

"Proteins, membranes and cells: the structure-function nexus". Contributions from the annual scientific meeting (including a special symposium in honour of Professor Alex Hope of Flinders University, South Australia) of the Australian Society for Biophysics held in Canberra, ACT, Australia, September 28–October 1, 2008.

P. Ju · J. I. Vandenberg (✉)
Division of Molecular Cardiology and Biophysics,
Victor Chang Cardiac Research Institute,
405 Liverpool Street, Darlinghurst, NSW 2010, Australia
e-mail: j.vandenberg@victorchang.edu.au

G. Pages · P. W. Kuchel · J. I. Vandenberg
School of Molecular and Microbial Biosciences,
University of Sydney, Sydney, NSW 2006, Australia

A. M. Torres
School of Biomedical and Health Sciences,
University of Western Sydney, Penrith South DC,
NSW 1797, Australia

P. S. Bansal
Australian Nuclear Science and Technology Organisation,
Lucas Heights, PMB 1, Menai, NSW 2234, Australia

P. F. Alewood
Institute for Molecular Bioscience, University of Queensland,
St. Lucia, QLD 4072, Australia

J. I. Vandenberg
St. Vincent's Clinical School, University of New South Wales,
Victoria Street, Darlinghurst, NSW 2010, Australia

Introduction

Ion channels are proteins that permit the selective flow of ions across cell membranes and are critical for electrical communication in many cell types. In the last decade the application of X-ray crystallography to the study of ion channels, and in particular K^+-selective bacterial ion-channels, has greatly enhanced the understanding of the overall architecture of the pore domains of this family of proteins and the mechanisms of ion selectivity. The

structural analysis of whole ion-channel proteins, however, is notoriously difficult (Rosenbusch et al. 2001), and with two notable exceptions (Long et al. 2005, 2007) has focused on bacterial ion-channel proteins because of the ease of over-expressing these in bacterial cultures.

The human *ether-a-go-go related* gene (hERG; Sanguinetti et al. 1995; Trudeau et al. 1995) encodes a voltage-gated K^+-selective ion channel that is crucial for repolarization of the cardiac action potential (Jurkiewicz and Sanguinetti 1993; Sanguinetti et al. 1995). Furthermore, mutations in hERG are responsible for ~35% of cases of the congenital long QT syndrome (LQTS; Splawski et al. 2000), an inherited arrhythmia syndrome that is associated with a markedly increased risk of sudden cardiac death (Keating and Sanguinetti 2001). The hERG K^+ channel shares a number of canonical features with other voltage-gated K^+ channels: they assemble as homo-tetramers with each subunit containing six transmembrane domains (denoted S1–S6; Fig. 1); the S1–S4 domains in each subunit form voltage sensor units (Bezanilla 2002) while the S5 and S6 domains along with the intervening pore loop from each of the four subunits form the ion conductance pathway (Yellen 2002). hERG however, also contains some unusual features, most notably a much longer pore-loop domain (Fig. 1b) than other K^+ channels.

In a previous study (Torres et al. 2003), we determined the structure of a peptide that corresponds to the S5P domain of hERG (from A570 to Y611), and showed that the region contains an amphipathic α-helix, from W585 to I593, that is important for the inactivation of hERG K^+ conduction. Furthermore, the peptide contains a second helical region at its C-terminus, corresponding to G604 to Y611. Based on sequence similarity to the pore helices of K^+ channels for which there are crystal structures, the pore-helix of hERG was predicted to run from Y611 to S621, thus a helical element from G604 to Y611, if contiguous with the pore-helix, would represent a significant N-terminal extension that would be unique amongst K^+ channels. Given the importance of the pore-helix for supporting the selectivity filter and thereby the inactivation of hERG K^+ channels (Vandenberg et al. 2004), it has been suggested that an extracellular extension of the pore-helix, through interactions with extracellular domains such as the S5P linker, may contribute to the uniquely rapid inactivation kinetics of hERG K^+ channels (Tseng et al. 2007). The peptide used in the previous study, however, did not contain the entire pore-helix and so it was not possible to form any firm conclusions about this putative pore-helix extension. Accordingly, the principal aim of the present study was to determine the length of the pore-helix of hERG.

We used NMR spectroscopy to study a 43-residue peptide (corresponding to S600-I642) that encompasses the predicted pore-helix (Y611-S621), as well as the putative extension (G604-Y611). The structure of this peptide was determined in sodium dodecyl sulfate (SDS) micelles, and dodecylphosphocholine (DPC) micelles. To identify the localization of residues inside the hydrophobic region, we used a water-soluble paramagnetic probe and studied the enhancement of relaxation rates of each amino acid residue (Ju et al. 2009; Zangger et al. 2008). The results indicated that the pore-helix of hERG, spanning K608 to S621, is indeed longer than the homologous helix in the K^+ channels for which crystal structures are known, although not as long as suggested in our previous study (Torres et al. 2003).

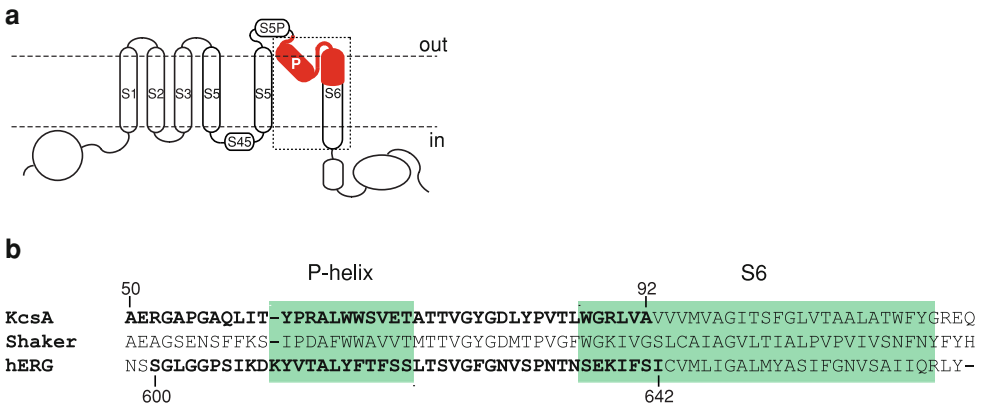

Fig. 1 Topology of hERG channels and alignment with related K^+ channels. **a** Predicted topology of a hERG K^+ channel subunit. The pore region is composed of the S5 and S6 domains and the intervening pore loop. *Dashed box* indicates region for which sequence alignment is provided in *panel* **b**. *Red* indicates the region corresponding to the peptide synthesized in this study. **b** Sequence alignment of the pore-helix, selectivity filter and the S6 regions of Shaker, KcsA and hERG (*boxed* in *panel* **a**) generated using ClustalW. *Green shading* indicates the predicted pore helices and S6 (shaker and hERG) or inner helix (KcsA). *Bold text* indicates hERG (S600-I642) and KcsA sequences (A50–A92) synthesized for NMR structure analysis (see text for details)

Materials and methods

NMR spectroscopy

The 43-residue hERG PS6 (4532.0 g/mol) and KcsA (4707.3 g/mol) peptides were synthesized on a 0.50 mmol scale using HBTU activation of Boc-amino acids with in situ neutralization chemistry, exactly as previously described (Schnölzer et al. 1992). The NMR spectroscopy sample consisting of ~2 mg of peptide (>99% purity) was dissolved in 400 µl of 90% H_2O:10% D_2O (v/v) containing either 100 mM ^{2}H-SDS or 100 mM ^{2}H-DPC (Cambridge Isotope Laboratories, Andover, MA, USA). The KcsA peptide was only studied in DPC micelles The paramagnetic relaxation agent gadolinium-diethylenetriamine pentaacetic acid-bismethylamide (a gift from Dr. Klaus Zangger, University of Graz, Graz, Austria) was introduced to both samples (SDS and DPC micelles) at a concentration of 2.4 mM.

NMR experiments were performed on a Bruker Avance-600 DRX spectrometer with a 5-mm triple resonance inverse cryoprobe with operating temperatures of 278, 298, 303, and 308 K. The two-dimensional (2D) experiments that were performed included double-quantum filtered correlation spectroscopy (DQF-COSY; Derome and Williamson 1990) with a phase cycle modified for fast recycle times (Derome and Williamson 1990); total correlation spectroscopy (TOCSY; Bax and Davis 1985) with MLEV spin-lock periods of 90 ms, and nuclear Overhauser enhancement spectroscopy (NOESY; Kumar et al. 1980) with mixing times of 200 and 250 ms. All 2D spectra were acquired using time-proportional phase detection (Marion and Wüthrich 1983) with 2 k data points in the direct dimension and usually 450 to 480 in the indirect dimension. Water-signal suppression in the NOESY experiment was achieved by low-power irradiation at the water resonance frequency during the relaxation delay of 1.3 s (pre-saturation) and during the mixing period; a SCUBA sequence (Brown et al. 1988) was also applied prior to the excitation pulse to reduce further the water signal and decrease the power of water irradiation during the relaxation delay. In DQF and TOCSY experiments solvent-signal suppression was achieved by applying either pre-saturation or WATERGATE (Piotto et al. 1992) pulse sequences. A hydrogen-deuterium exchange experiment was carried out by adding D_2O to a freeze-dried NMR sample and acquiring a series of 1D experiments for 1 h followed by a 5 h TOCSY experiment.

All spectra were processed using XWIN-NMR software (Bruker) and were analysed using the standard protocol in the program XEASY (Bartels et al. 1995). To analyse the effect of the paramagnetic relaxation molecule, rectangles were drawn around each intra-residue labelled peak in the NOESY experiments. Integration of cross-peaks was performed for all rectangles using the same contour level for both experiments before and after the addition of the paramagnetic molecule. The average signal attenuation was calculated for each residue and results were normalized to have a maximum residual signal value of 100% (equivalent to no effect of the paramagnetic molecule).

Structure calculations

Distance constraints were obtained from cross-peak volumes in the NOESY spectra that had been recorded with a mixing time of 200 ms at 298 K. The data from PS6 in DPC micelles provided 463 non-redundant upper-distance constraints. An additional ten distant constraints for H-bonding were obtained from a hydrogen-deuterium exchange experiment, and after analysis of medium-resolution structures. No ϕ dihedral angle constraints were deduced from the spectra because the backbone amide peaks were too broad to allow measurement of these; the line-broadening was likely to have been caused by slow conformational averaging of the peptide structures in the presence of the micelles. In the initial stages of structure calculations, the NOAH protocol (Mumenthaler and Braun 1995; Mumenthaler et al. 1997) in the torsion-angle dynamics program DYANA (Güntert et al. 1997) was implemented to aid in identifying cross-peaks and in obtaining additional NOE constraints. The standard simulated annealing protocol in DYANA was then used to improve the quality of structures and to obtain further constraints. The final PS6 structures presented here were obtained using the standard dynamic annealing protocol, anneal.inp, in the program CNS (Brünger et al. 1998). The high temperature dynamics and cooling cycle were performed in torsion-angle space. An extended conformation of PS6 was used as a starting point to generate 500 structures from which the 'best' 20, with lowest overall energy, were selected and considered as representative structures of PS6.

Results

PS6 structure in DPC micelles

The amide region of the 200 ms mixing-time NOESY spectrum of PS6 in DPC micelles, at 298 K, is shown in Fig. 2a; and the NMR structural data for PS6 in DPC micelles are summarized in Fig. 2b. The presence of NOESY cross-peaks in the amide region of the NOESY spectrum suggested turn-like or helical conformation in the molecule (Fig. 2a). Furthermore, the presence of NOE connectivities $\delta\alpha\beta$(i, i + 3) and/or $\delta\alpha$N(i, i + 3) spanning

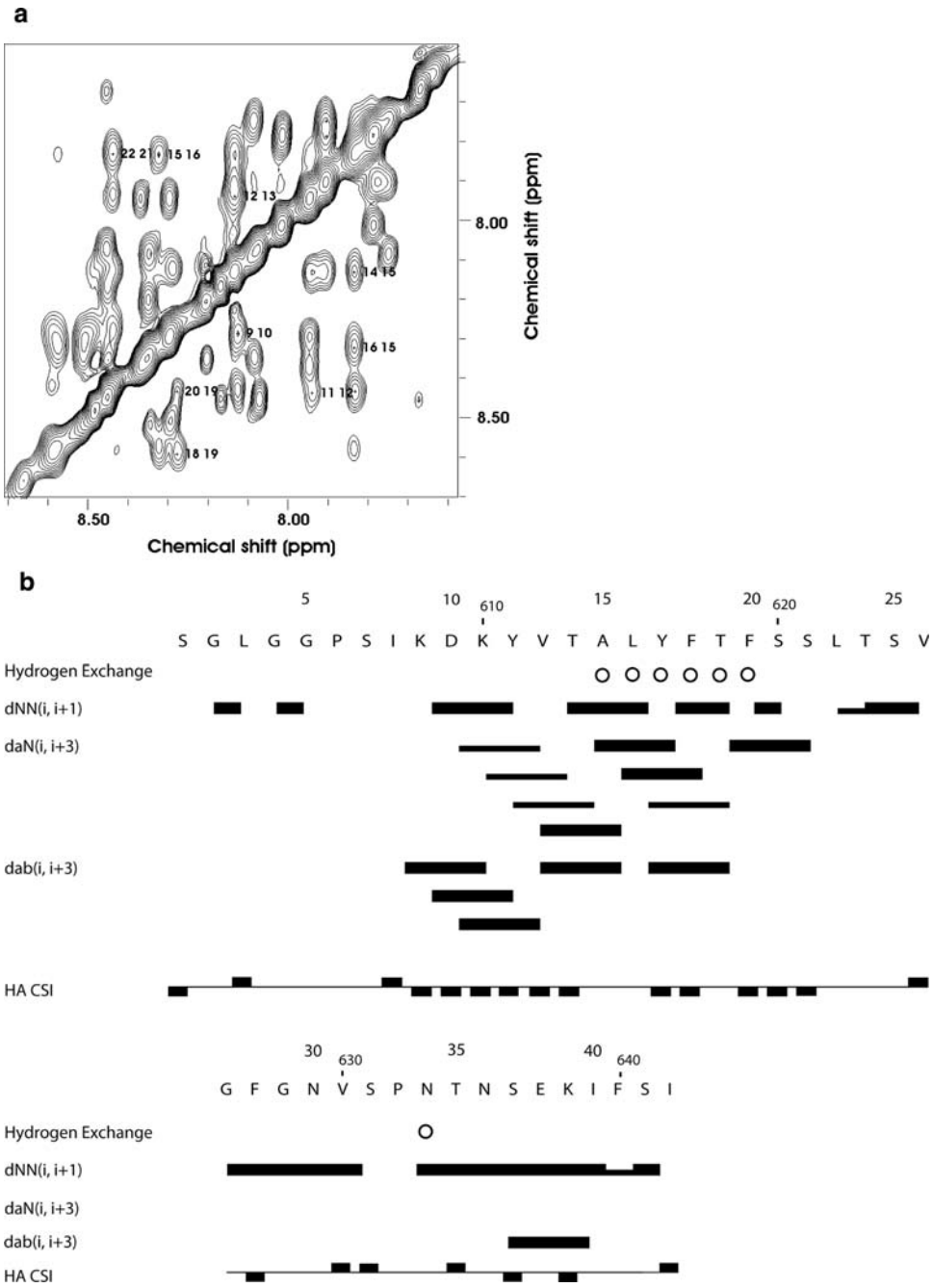

Fig. 2 ^{1}H NMR analysis of hERG PS6 peptide in 100 mM DPC at pH 3.4 and 298 K. **a** ^{1}H NMR amide region of 200 ms mixing time NOESY spectrum. The presence of NOESY cross-peaks in this region suggests turn-like or helical conformation in the molecule. The intense cross-peaks in the spectrum are labelled with the residue numbers corresponding to the two amide protons that are close in space. **b** Summary of NMR data of PS6 peptide in 100 mM DPC. Peptide residue numbers corresponding to *panel* **a** and equivalent residue numbers are shown above the sequence. Slowly exchanging backbone amide protons are indicated by *circles*. NOE connectivities that indicate close through-space interactions are represented by *shaded horizontal bars* whose thicknesses are proportional to the observed NOE intensities. The CSI plot for each residue is indicated by *positive or negative vertical bars* indicating whether the chemical shift was deviated in a positive or negative direction compared to that expected for a residue in a random coil. The break in amide-amide connectivity in the diagram was likely to be superficial and due to peak overlap

residues 9–22 (equivalent to K608 to S621) indicated the presence of an α-helix in this region. The presence of additional δNN(i, i + 1) NOEs spanning residues equivalent to L622-S624 suggests the presence of a turn-like conformation in this part of the molecule. Lastly, contiguous negative chemical shift index (CSI) values for residues in this region also supports the presence of a helical structure spanning residues equivalent to K608 to S621. The slowly exchanging backbone amide protons, as found for residues equivalent to A614-F619, suggested hydrogen-bonding with the backbone carbonyl oxygen of amino-acids that were likely to be parts of the same helix. It is possible that some amide residues, K608-T613, were also hydrogen-bonded but these were not unambiguously assigned due to peak overlap. The NOE connectivities observed for PS6 were exclusively intra-residual, sequential, and medium-range (Table 1). The absence of long-range NOEs suggests that this 43-residue peptide is relatively flexible and has no defined *tertiary* structure in DPC micelles.

Figure 3a shows the ensemble of 20 calculated PS6 structures superimposed over the backbone of the well-defined region of residues equivalent to K608-S624. It is

Table 1 Structural statistics for 20 PS6 peptide structures

Quantity	Value
Distance restraints	
Intraresidue ($i - j = 0$)	194
Sequential ($\|i - j\| = 1$)	161
Medium-range ($\|i - j\| \leq 5$)	108
Long-range ($\|i - j\| \geq 5$)	0
Hydrogen-bonds	10
Total	473
Mean energies (kcal mol^{-1})	
E_{NOE}	1.65 ± 0.63
E_{vdW}	6.26 ± 0.83
E_{bond}	0.55 ± 0.10
$E_{improper}$	0.84 ± 0.10
E_{angle}	17.95 ± 0.37
E_{total}	27.26 ± 1.28
Atomic rms difference with the mean (Å)	
Backbone atoms (8–24) (I607-L623)	0.71 ± 0.25
Heavy atoms (8–24) (I607-L623)	1.14 ± 0.27
Backbone atoms (9–21) (K608-S620)	0.29 ± 0.20
Heavy atoms (9–21) (K608-S620)	0.85 ± 0.25

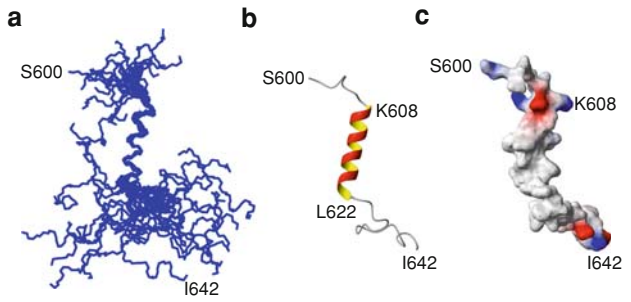

Fig. 3 NMR-based structure of PS6 peptide in DPC micelles. **a** The ensemble of 20 calculated PS6 peptide structures superimposed over the backbone atoms of residues equivalent to I607 to T623 of the local mean structure. **b** A ribbon diagram of one structure showing an α-helix at residues equivalent to K608-L622. **c** Potential surface diagram for the structure shown in panel **b** Positively charged side-chains are shown in *blue* and negatively charged side chains in *red*. The diagrams were generated using the program MOLMOL (Koradi et al. 1996)

important to point out that while the well-defined helical region always spanned residues K608-S621 in some of the lowest energy structures the helix was shortened or extended by one residue (e.g. see Fig. 3c). For the backbone the root mean square deviation was 0.71 Å for the well-defined region, and 0.29 Å for the helix (Table 1). The N-terminal region up to the residue equivalent to I607, and the *C*-terminal region from residue V625, were flexible and did not appear to have any localized well-defined structure. A potential surface diagram for the structure shown in Fig. 3b is shown in Fig. 3c and highlights the highly charged motif (KDK) at the N-terminal end of the pore-helix.

PS6 structure in SDS micelles

We also investigated whether the length of the pore-helix in hERG was dependent on the type of micelles used. When the hERG peptide was dissolved in SDS micelles the peptide showed limited solubility; consequently the resolution of the calculated structure in SDS micelles was relatively low. Nevertheless, the CSI plot clearly indicated that the hERG peptide in SDS micelles had a well-defined α-helix in the pore region that covered the same region of the peptide as that seen in DPC micelles (Fig. 4a). Thus the longer pore-helix seen in the hERG peptide was not micelle-specific.

Positioning of PS6 in DPC and SDS micelles

To localize residues outside DPC and SDS micelles, we added a gadolinium-based paramagnetic relaxation agent to the peptide/micelle mixtures. The paramagnetic molecule enhances the relaxation rates of protein protons as a function of their surface exposure and distance from the surface. Because gadolinium complexes are water-soluble, the only relaxation enhancement rates (and hence signal attenuation) are observed for residues in the hydrophilic environment, outside micelles (Ju et al. 2009; Pintacuda and Otting 2002; Respondek et al. 2007; Zangger et al. 2008).

Figure 4b shows the normalized residual signals after addition of the paramagnetic molecule for each residue in both DPC and SDS micelles. A low residual signal is obtained for significantly enhanced relaxation rate of a specific residue due to the gadolinium, namely for residues located outside the micelle. In the presence of SDS, a high residual signal was measured from residues equivalent to I607 to G626, and possibly F627. The peptide was situated inside the micelle one residue before the N-terminal end of the helix and two or three residues after the *C*-terminal end of the helix/turn-like structure. It is interesting to note that the side chain of the residue equivalent to K610 and aromatic protons from both F617 and F619 had a low residual signal, contrasting with the backbone signal attenuations of these residues. These residues are therefore likely to be located at the border, or close to the border, of the hydrophobic/hydrophilic region.

For DPC micelles, residues equivalent to I607 and K608 showed medium residual signal intensity indicating that these residues could penetrate at least partially into the surface of the micelle whereas D609 was definitely in a hydrophilic environment, outside the micelle. From residues equivalent to K610 to F627 or possibly G628, NMR

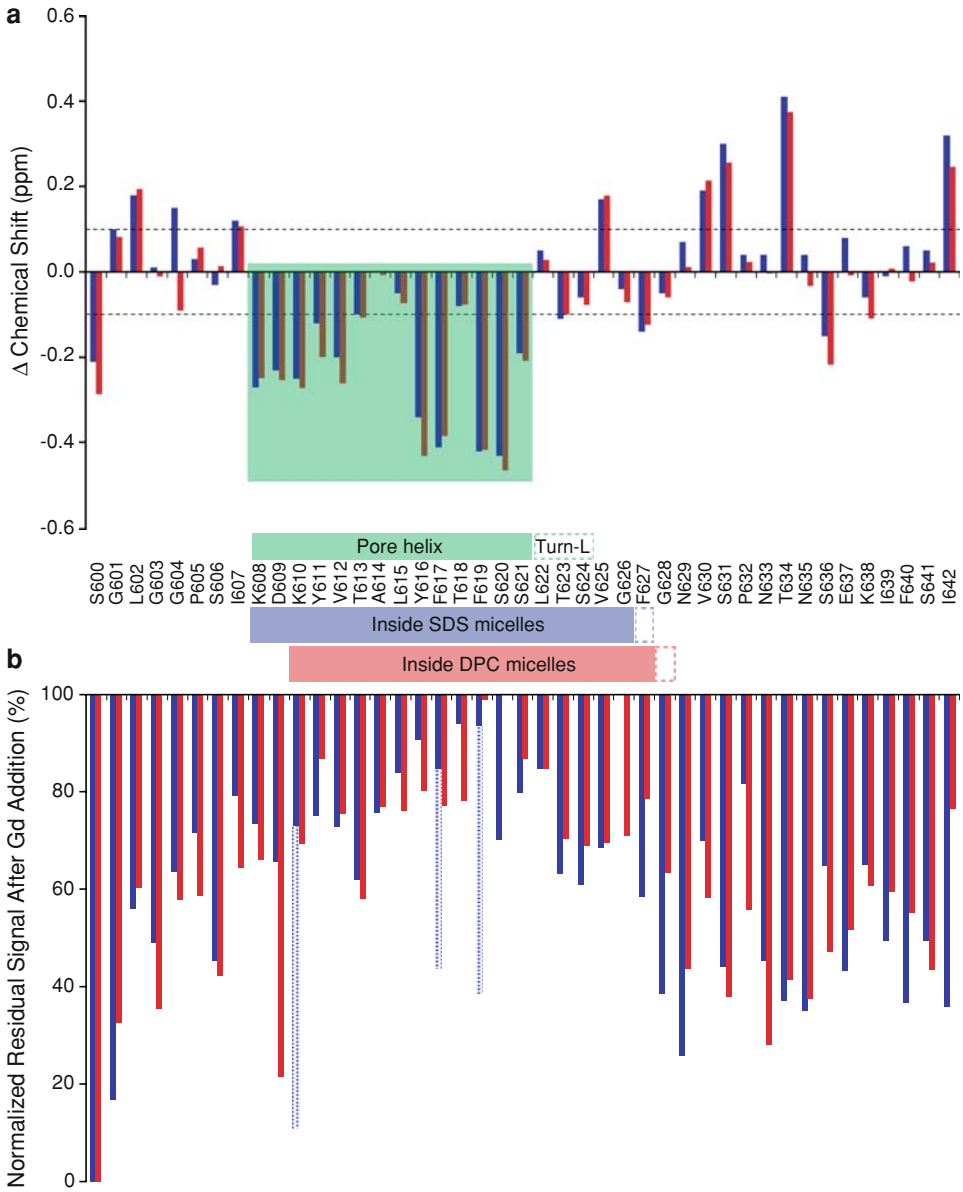

Fig. 4 Comparison of hERG peptide properties in SDS (*blue*) and DPC (*red*) micelles. **a** The chemical shift for the Cα proton plotted as a deviation from the value expected for that residue in a random coil. Values of ±0.1 ppm, considering has a characteristic deviation, are represented by *dashed lines*. Continuous stretches of negative chemical shift values are strongly indicative of an α-helical structure (highlighted by *green shading*). **b** Normalized residual signal after addition of the gadolinium-based relaxant agent. A series of high residual values (short length histograms) is observed between K608 and G628 depending on the micelles. The *blue dotted histograms* show side chains attenuations that are significantly different from the backbone attenuations. *Blue and red boxes* show residues inside SDS and DPC micelles, respectively. *Dashed boxes* show a possible extension inside micelles

signal attenuation was low, characterizing residues inside the micelle. Thus, whereas in SDS micelles the entire pore helix-turn motif appeared to be within the micelle, in DPC micelles at least three residues at the N-terminal end of the pore-helix were exposed to the hydrophilic environment outside the micelle.

Pore-helix length in hERG PS6 compared with KcsA PS6

The pore-helix in the hERG PS6 peptide was longer than that predicted by comparison with the crystal structures of K^+ channels (see Fig. 5c, below). It is conceivable that this could be an artefact of studying the peptide in a micelle environment, rather than in the native channel where it would be surrounded by other protein domains and the lipid bilayer. To investigate whether this might be the case we studied a homologous peptide from KcsA (A50–A92) in DPC micelles, and compared its structure to that obtained by X-ray crystallography of the full-length channel. The resonances for KcsA were relatively broad, thus despite the clear presence in the spectra of amide-amide connectivities it was difficult to identify sequential NOEs (data not shown). Nevertheless, the stretch of negative CSI values (see Fig. 5b) indicated the presence of an α-helical region that starts at the residue equivalent to T61 and extends to S69 and possibly as far as T74. In the different KcsA crystal structures available in the protein data

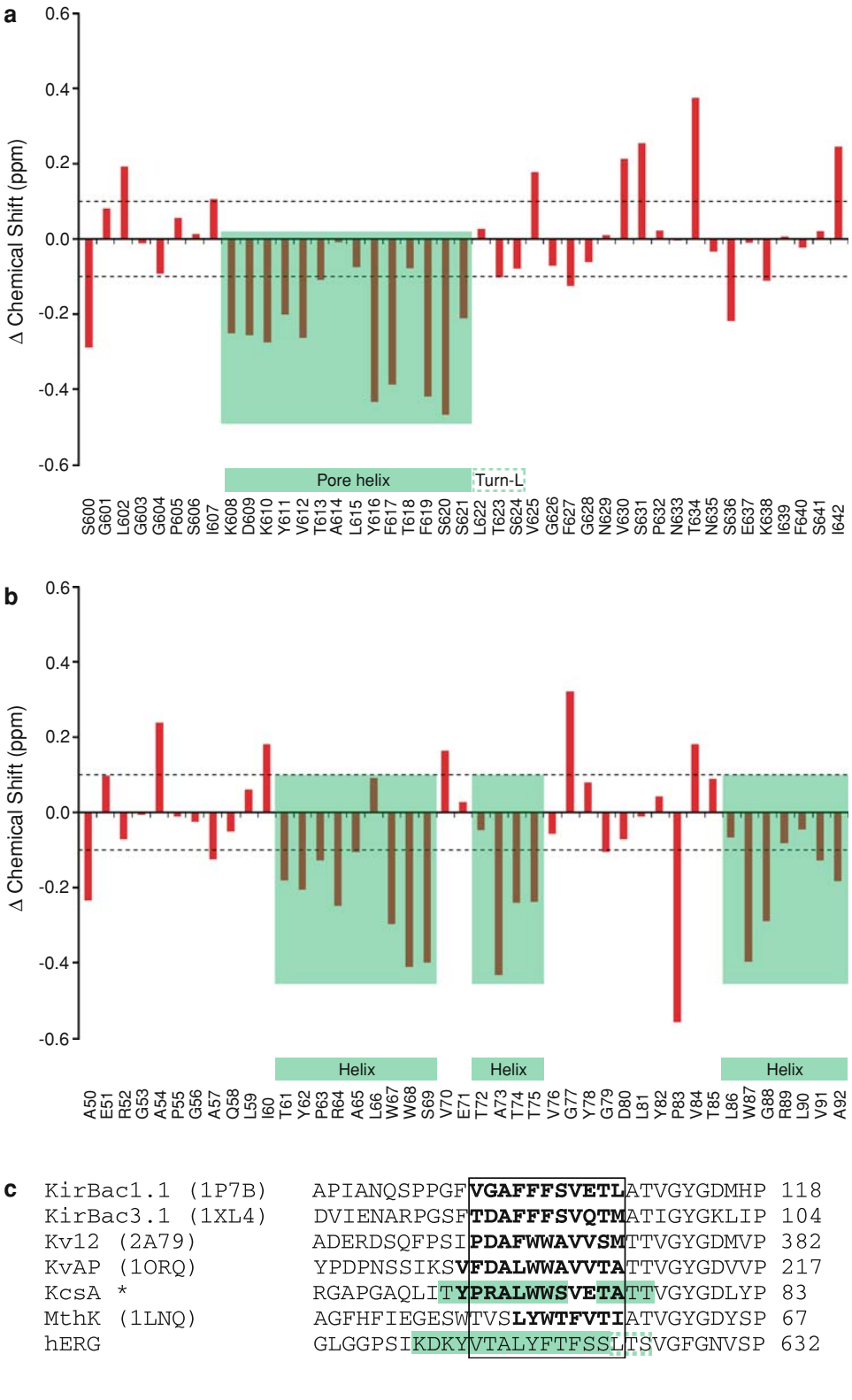

Fig. 5 Comparison of chemical shift deviations for hERG and KcsA pore-helix peptides in DPC micelles. Absolute changes in chemical shift for the Cα-protons, relative to those expected for a random coil for **a** hERG peptide in DPC micelles and **b** KcsA peptide in DPC micelles. *Green shaded boxes* indicate putative helical regions. **c** Sequence alignment of the pore-helix region of hERG with the pore-helix regions of the K^+ channels, for which crystal structures are known. Codes shown in parentheses are the protein data bank codes for the corresponding crystal structures (www.pdb.org). *Asterisk* indicates data shown for KcsA are the consensus derived from the multiple crystal structures available in the protein database (see text for details). *Bold letters* indicate residues in pore-helix in crystal structure, *boxed region* represents consensus for pore-helix region, *green shading* indicates helical regions from NMR studies of isolated peptides

bank, the pore-helix is most commonly reported to start at Y62 and to finish at either A73 or T74 (see e.g. 1r3k.pdb and 1k4c.pdb). Thus overall the length of the pore-helix predicted from our NMR studies in the presence of DPC micelles is very similar to that reported by crystallographic studies of the full-length channel. Therefore, at least in the case of KcsA, removing the pore-helix from its native protein/bilayer environment does not appear to perturb the

extent of the helix. One discrepancy between the structural predictions for the pore-helix of KcsA reported here and the X-ray crystallography data is the presence of an apparent break in the helix at residues equivalent to V70-E71 in the NMR data. E71 is known to interact with D80 just beyond the selectivity filter in the intact channel (Cordero-Morales et al. 2007). We suggest that the E71-D80 interaction may not be present in our experiments and this could perturb the calculated local structure.

Discussion

Based on the sequence homology and functional similarity to KcsA, KvAP, MthK, Kv1.2 and KirBac1.1 (i.e. K^+ selectivity) the PS6 peptide studied here was predicted to contain a pore-helix for residues equivalent to Y611-S621. In contrast, the peptide adopted a helical conformation extending from residues equivalent to K608-S621. In a previous study of a peptide spanning the S5P region of hERG (Torres et al. 2003) we suggested that the pore-helix may be extended at its N-terminal end (by up to seven residues). This suggestion has since been incorporated into structural models of the hERG pore domain (see e.g. Stansfeld et al. 2007; Tseng et al. 2007). However, based on the results from the present study we believe the pore-helix is extended by only three residues at its N-terminal end. There are two observations that indicate that the results from the present study are more reliable than the previous study. First, the peptide used in the previous study did not span the entire putative pore-helix region, whereas the peptide used here does. Second, the length of the pore-helix found in a peptide from KcsA, homologous to the hERG peptide used in this study, was very similar to that seen in the crystal structures of KcsA (Doyle et al. 1998); thus we can be reasonably confident that the longer helix seen in the present hERG peptide is not simply an artefact of studying the peptide isolated from its native protein/lipid environment. Note that structures of membrane associated proteins determined by NMR and X-ray crystallography are not always folded identically, e.g. for the case of the N-terminus of the toxin EqtII, Drechsler et al. (2006), report a significant extension of the helix of the peptide in SDS micelles compared to the crystal structure of the protein. However, this does not appear to be the case for the pore-helix domain of the KcsA K^+ channel and therefore we propose that it is unlikely to apply to the hERG pore-helix domain.

In addition to the pore-helix, the peptides analysed in this study also contained the selectivity filter as well as the N-terminal seven residues of the S6 helix. Neither of these elements were well resolved in either the hERG peptide or KcsA peptide. The absence of the S6 helix in PS6 is not surprising since only a small part (7 out of 28 residues) of the predicted S6 helix was included in the synthesized peptide. The orientation of the pore-helix, relative to the S6 helix, is important in defining the conformation of the tight loop that includes the selectivity filter. Thus the absence of a second helix (S6) in PS6, as determined in this study, could explain the lack of structural definition in the predicted selectivity filter. Nevertheless, the clear difference in the extent of the pore-helix seen in the hERG peptide, compared with the KcsA peptide where the helix length is very similar to that seen in the crystal structures, is consistent with hERG channels containing a longer pore-helix. Furthermore, based on the sequence homology at the *C*-terminal end of the hERG and KcsA pore helices, and the clear importance of the position of the *C*-terminal end of the pore-helix for K^+ channel function (Doyle et al. 1998), we suggest that a longer pore-helix in hERG would be accommodated by an extension at the N-terminal end projecting into the extracellular space.

To check this last hypothesis, we localized residues inside each micelle using a gadolinium-based relaxation agent. While for SDS, that is anionic, residues are in the hydrophobic region one residue before (I607) the N-terminal end of the helix and two or three residues after (G626 or F627) the C-terminal helical end; in the zwitterionic micelle (DPC) not all residues of the helix are located within the hydrophobic region of the micelle. The residue equivalent to D609 is situated outside the micelles while residues equivalent to I607 and K608 could be at the boundary between both hydrophobic and hydrophilic regions. The presence of phosphocholine head groups on DPC is expected to more closely simulate a membrane interface than in a SDS micelle environment. Furthermore, a difference in the penetration depth inside a micelle is suspected. In SDS, relaxation rates for the side chains on residues equivalent to K610, F617 and F619 are enhanced suggesting localization in a hydrophilic environment, i.e. at the border of the SDS micelle. This is not the case with a DPC micelle; suggesting that in the of DPC micelles K610, F617 and F619 are all within the micelle thus escaping any paramagnetic effect.

The two main difference between both types of micelles deals with NMR spectral resolution and relative position of the pore-helix in the micelles. In the presence of DPC, it was possible to calculate a high-resolution structure of the peptide while in an SDS environment, the calculated structure had a much lower resolution. Despite only being able to calculate a low-resolution structure in SDS micelles, it is clear from the CSI plots, that the helical structure for both environments spanned the same region of the peptide suggesting that the peptide had a similar configuration. In the anionic SDS micelles the N-terminal end of the helix (starting at residue K608) appeared to be

anchored at the water-micelle interface whereas in the zwitterionic DPC micelles the residues equivalent to K608 (N-terminal end of the helix) as well as D609 appeared to be located outside the micelle. This difference in the anchor point for a peptide in different micelle environments is similar to that reported by (de Planque et al. 1999). Given that mammalian membranes contain predominantly lipids with zwitterionic headgroups we propose that the pore-helix in cells is likely to protrude into the extracellular space analogous to what we have observed for the pore-helix peptide in DPC micelles.

In conclusion, we have shown that the α-helix in the pore loop domain of the hERG channel (K608-S621) is longer at its N-terminus by ~3 residues, compared with the homologous helix in the K^+ channels, for which crystal structures are known (Fig. 5). This outcome differs from our previous findings on the hERG S5P peptide (A570-Y611; Torres et al. 2003) where we suggested that the pore-helix may be up to seven residues longer than the equivalent helix in other K^+ channels. We contend that the present NMR data are less ambiguous than in the previous study, regarding the pore-helix. We have demonstrated that the extent of incorporation of the hERG pore-helix peptide inside a micelle (SDS or DPC) is micelle-dependent. In the DPC micelles, where the phosphocholine headgroup more closely approximates that seen in eukaryotic-membranes, the extension at the N-terminal end of the pore-helix projects outside the micelle as shown by the paramagnetic relaxation enhancement on the terminal amino acid residues. A comparison of the hERG and KcsA pore-helix peptides revealed that the continuous pore-helix in hERG is longer than that seen in KcsA (Fig. 5c) and we postulate that this would also apply in native membrane environments. Ultimately, this will require confirmation using the structure of the entire hERG channel in as close to a native environment as possible by, most probably, X-ray crystallography.

Given the importance of the pore-helix for supporting the selectivity filter and thereby the inactivation of hERG K^+ channels (Vandenberg et al. 2004), we suggest that an extracellular extension of the pore-helix, through interactions with extracellular domains such as the S5P linker, may contribute to the uniquely rapid inactivation kinetics of hERG K^+ channels. This proposal awaits experimental testing.

Acknowledgments We thank Sue Ku and Tadeusz Marciniec for expert technical assistance and Adam Hill and Catherine Clarke for valuable discussions. JIV was supported by a National Health and Medical Research Council Senior Research Fellowship (459401) and PWK was supported by an Australian Research Council Australian Professorial Fellowship (DP0345961). This work was also supported in part by grants from the NH&MRC (459402 to JIV), ARC (DP0440808 to PWK and JIV) and a New South Wales Health Research and Development infrastructure grant.

References

Bartels C, Xia T-H, Billeter M, Güntert P, Wüthrich K (1995) The program XEASY for computer-supported NMR spectral analysis of biological macromolecules. J Biomol NMR 6:1–10. doi:10.1007/BF00417486

Bax A, Davis DG (1985) MLEV-17-based two-dimensional homonuclear magnetization transfer spectroscopy. J Magn Reson 65:355–360

Bezanilla F (2002) Voltage sensor movements. J Gen Physiol 120:465–473. doi:10.1085/jgp.20028660

Brown SC, Weber PL, Mueller L (1988) Toward complete ^{1}H NMR spectra in proteins. J Magn Reson 77:166–169

Brünger AT, Adams PD, Clore GM, DeLano WL, Gros P, Grosse-Kunstleve RW, Jiang J-S, Kuszewski J, Nilges M, Pannu NS, Read RJ, Rice LM, Simonson T, Warren GL (1998) Crystallography & NMR system: a new software suite for macromolecular structure determination. Acta Crystallogr D Biol Crystallogr 54:905–921. doi:10.1107/S0907444998003254

Cordero-Morales JF, Jogini V, Lewis A, Vasquez V, Cortes DM, Roux B, Perozo E (2007) Molecular driving forces determining potassium channel slow inactivation. Nat Struct Mol Biol 14:1062–1069. doi:10.1038/nsmb1309

de Planque MR, Kruijtzer JA, Liskamp RM, Marsh D, Greathouse DV, Koeppe REII, de Kruijff B, Killian JA (1999) Different membrane anchoring positions of tryptophan and lysine in synthetic transmembrane alpha-helical peptides. J Biol Chem 274:20839–20846. doi:10.1074/jbc.274.30.20839

Derome AE, Williamson MP (1990) Rapid-pulsing artifacts in double-quantum-filtered COSY. J Magn Reson 88:177–185

Doyle DA, Cabral JM, Pfuetzner RA, Kuo A, Gulbis JM, Cohen SL, Chait BT, MacKinnon R (1998) The structure of the potassium channel: molecular basis of K^+ conduction and selectivity. Science 280:69–77. doi:10.1126/science.280.5360.69

Drechsler A, Potrich C, Sabo JK, Frisanco M, Guella G, Dalla Serra M, Anderluh G, Separovic F, Norton RS (2006) Structure and activity of the N-terminal region of the eukaryotic cytolysin equinatoxin II. Biochemistry 45:1818–1828. doi:10.1021/bi052166o

Güntert P, Mumenthaler C, Wüthrich K (1997) Torsion angle dynamics for NMR structure calculation with the new program DYANA. J Mol Biol 273:283–298. doi:10.1006/jmbi.1997.1284

Ju P, Pages G, Riek RP, Chen P-C, Torres AM, Bansal PS, Kuyucak S, Kuchel PW, Vandenberg JI (2009) The pore domain outer helix contributes to both activation and inactivation of the hERG K^+ channel. J Biol Chem 284:1000–1008. doi:10.1074/jbc.M806400200

Jurkiewicz NK, Sanguinetti MC (1993) Rate-dependent prolongation of cardiac action potentials by a methanesulfonanilide class III antiarrhythmic agent. Specific block of rapidly activating delayed rectifier K^+ current by dofetilide. Circ Res 72:75–83

Keating MT, Sanguinetti MC (2001) Molecular and cellular mechanisms of cardiac arrhythmias. Cell 104:569–580. doi:10.1016/S0092-8674(01)00243-4

Koradi R, Billeter M, Wüthrich K (1996) MOLMOL: a program for display and analysis of macromolecular structures. J Mol Graph 14:51–55. doi:10.1016/0263-7855(96)00009-4

Kumar A, Ernst RR, Wüthrich K (1980) A two-dimensional nuclear Overhauser enhancement (2D NOE) experiment for the elucidation of complete proton-proton cross-relaxation networks in biological macromolecules. Biochem Biophys Res Commun 95:1–6. doi:10.1016/0006-291X(80)90695-6

Long SB, Campbell EB, MacKinnon R (2005) Crystal structure of a mammalian voltage-dependent shaker family K^+ channel. Science 309:897–903. doi:10.1126/science.1116269

Long SB, Tao X, Campbell EB, MacKinnon R (2007) Atomic structure of a voltage-dependent K^+ channel in a lipid membrane-like environment. Nature 450:376–382. doi:10.1038/nature06265

Marion D, Wüthrich K (1983) Application of phase sensitive two-dimensional correlated spectroscopy (COSY) for measurements of 1H–1H spin-spin coupling constants in proteins. Biochem Biophys Res Commun 113:967–974. doi:10.1016/0006-291X(83)91093-8

Mumenthaler C, Braun W (1995) Automated assignment of simulated and experimental NOESY spectra of proteins by feedback filtering and self-correcting distance geometry. J Mol Biol 254:465–480. doi:10.1006/jmbi.1995.0631

Mumenthaler C, Güntert P, Braun W, Wüthrich K (1997) Automated combined assignment of NOESY spectra and three-dimensional protein structure determination. J Biomol NMR 10:351–362. doi:10.1023/A:1018383106236

Pintacuda G, Otting G (2002) Identification of protein surfaces by NMR measurements with a paramagnetic Gd(III) chelate. J Am Chem Soc 124:372–373. doi:10.1021/ja016985h

Piotto M, Saudek V, Sklenář V (1992) Gradient-tailored excitation for single-quantum NMR spectroscopy of aqueous solutions. J Biomol NMR 2:661–665. doi:10.1007/BF02192855

Respondek M, Madl T, Göbl C, Golser R, Zangger K (2007) Mapping the orientation of helices in micelle-bound peptides by paramagnetic relaxation waves. J Am Chem Soc 129:5228–5234. doi:10.1021/ja069004f

Rosenbusch JP, Lustig A, Grabo M, Zulauf M, Regenass M (2001) Approaches to determining membrane protein structures to high resolution: do selections of subpopulations occur? Micron 32:75–90. doi:10.1016/S0968-4328(00)00021-4

Sanguinetti MC, Jiang C, Curran ME, Keating MT (1995) A mechanistic link between an inherited and an acquird cardiac arrthytmia: hERG encodes the IKr potassium channel. Cell 81:299–307. doi:10.1016/0092-8674(95)90340-2

Schnölzer M, Alewood P, Jones A, Alewood D, Kent S (1992) In situ neutralization in Boc-chemistry solid phase peptide synthesis. Int J Pept Protein Res 40:180–193

Splawski I, Shen J, Timothy KW, Lehmann MH, Priori S, Robinson JL, Moss AJ, Schwartz PJ, Towbin JA, Vincent GM, Keating MT (2000) Spectrum of mutations in long-QT syndrome genes : KVLQT1, hERG, SCN5A, KCNE1, and KCNE2. Circulation 102:1178–1185

Stansfeld PJ, Gedeck P, Gosling M, Cox B, Mitcheson JS, Sutcliffe MJ (2007) Drug block of the hERG potassium channel: insight from modeling. Proteins 68:568–580. doi:10.1002/prot.21400

Torres AM, Bansal PS, Sunde M, Clarke CE, Bursill JA, Smith DJ, Bauskin A, Breit SN, Campbell TJ, Alewood PF, Kuchel PW, Vandenberg JI (2003) Structure of the hERG K^+ channel S5P extracellular linker: role of an amphipathic α-helix in C-type inactivation. J Biol Chem 278:42136–42148. doi:10.1074/jbc.M212824200

Trudeau MC, Warmke JW, Ganetzky B, Robertson GA (1995) hERG, a human inward rectifier in the voltage-gated potassium channel family. Science 269:92–95. doi:10.1126/science.7604285

Tseng G-N, Sonawane KD, Korolkova YV, Zhang M, Liu J, Grishin EV, Guy HR (2007) Probing the outer mouth structure of the hERG channel with peptide toxin footprinting and molecular modeling. Biophys J 92:3524–3540. doi:10.1529/biophysj.106.097360

Vandenberg JI, Torres AM, Campbell TJ, Kuchel PW (2004) The HERG K+ channel: progress in understanding the molecular basis of its unusual gating kinetics. Eur Biophys J 33:89–97. doi:10.1007/s00249-004-0419-y

Yellen G (2002) The voltage-gated potassium channels and their relatives. Nature 419:35–42. doi:10.1038/nature00978

Zangger K, Gößler R, Khatai L, Lohner K, Jilek A (2008) Structures of the glycine-rich diastereomeric peptides bombinin H2 and H4. Toxicon 52:246–254. doi:10.1016/j.toxicon.2008.05.011